EVIDENCE FOR NEUTRINO OSCILLATIONS AT LSND

Eric D. Church
University of California, Riverside, CA 92521
echurch@lanl.gov,

representing the LSND collaboration.

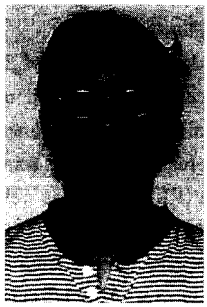

Abstract

Searches for $\nu_\mu \to \nu_e$[1] and $\overline{\nu}_\mu \to \overline{\nu}_e$[2] oscillations with the LSND experiment[3] at the Los Alamos Meson Physics Facility have been performed using ν_μ from π^+ decay in flight (DIF) and $\overline{\nu}_\mu$ from μ^+ decay at rest (DAR), respectively. The DIF (DAR) analysis finds an oscillation probability of $(2.6 \pm 1.0)\times 10^{-3}$ ($(3.1 \pm 1.2)\times 10^{-3}$), with a probability of statistical fluctuation equal to $\sim 1.1 \times 10^{-3}$ (4.1×10^{-8}). The most-favored Δm^2 range, taking into account results at all experiments, is $0.2 \lesssim \Delta m^2 \lesssim 2$ eV^2. The LSND experiment and the above-mentioned analyses are discussed here.

1 Introduction

The main source of DIF (DAR) ν_μ ($\overline{\nu}_\mu$) for this experiment is the A6 water target of the LAMPF 800 MeV proton linear accelerator. Approximately 3.4% of the π^+ produced in the 30 cm target decay in flight before reaching the water-cooled copper beam stop, roughly 1.5m downstream, to give the DIF flux. The remainder of the π^+ decay at rest to μ^+, nearly all of which decay at rest to give the DAR flux. Two upstream thin carbon targets, A1 and A2, located 135m and 110 m upstream from the detector center, respectively, provide additional small contributions to the fluxes, which however may be significant for the DIF analysis if Δm^2 is small, due to the long baselines. The LSND measurement [4] of the exclusive reaction $\mu^{-12}\mathrm{N}_{g.s.}$, with its well-understood cross section, confirms the DIF flux to within a 15% error, while the LSND measurement [5] of the $\nu_e C$ cross section fixes the DAR flux to within a smaller error.

The data taken for the two analyses reported here comes from runs taken in 1993, 1994 and 1995, with total charges delivered to the beam stop of 1787 C, 5904 C and 7081 C. Preliminary results from 1996-1997 data are also shown.

The detector is a tank filled with 167 metric tons of dilute liquid scintillator, located 30m downstream from the neutrino source and surrounded on all sides except the bottom by a liquid scintillator veto shield. The dilute mixture allows detection in the surrounding 1220 tank photomultiplier tubes of both Čerenkov light and scintillation light, so that reconstruction provides robust particle identification (PID) for $e^\pm$, as well as the direction and position of the $e^\pm$.

Despite 2.0 kg/cm^2 shielding above the detector tunnel, there remains a large background to the oscillation search due to cosmic rays. The background is highly suppressed by a veto shield [6] which provides active and passive shielding. If six or more of the 292 veto tubes fired in one 100 nsec interval, a signal holds off the trigger for 15.2 μsec. An 18% cost in dead-time is incurred due to the veto hold-off, while a veto inefficiency of $< 10^{-5}$ is achieved off-line for incident charged particles. The veto inefficiency is much larger for incident cosmic-ray neutrons.

The data acquisition and triggering do not depend on whether the beam is on or off, thus the beam-on to beam-off duty ratio can be measured for triggered events; it averaged 0.070 ± 0.001 over the three years of data on which these results are reported. The beam-unrelated background in any beam-on sample is thus well measured from the much larger beam-off sample and can be subtracted. Still, the cuts used to select $e^\pm$ in the two analyses are designed to discriminate heavily against this background so that the statistical error from the subtraction may be kept small relative to the beam-dependent signal.

2 Analysis: DAR

A DAR oscillation event signature consists of an "electron" signal followed by a 2.2 MeV photon correlated with the electron in both position and time. Detection of DAR ν_e is dominated in LSND by charge current reactions on ^{12}C. However, electrons from $\nu_e^{12}C \rightarrow e^{-12}N$ have energy

E_e < 36 MeV. Moreover, DAR production of a correlated photon from $\nu_e^{12}C \rightarrow e^- n^{11}N$ can only occur for E_e < 20 MeV.

PID in the DAR analysis is achieved in a straightforward way [2] which exploits the differences in the position, timing and angle distributions in events with particles above and below Čerenkov threshold. See figure 1.

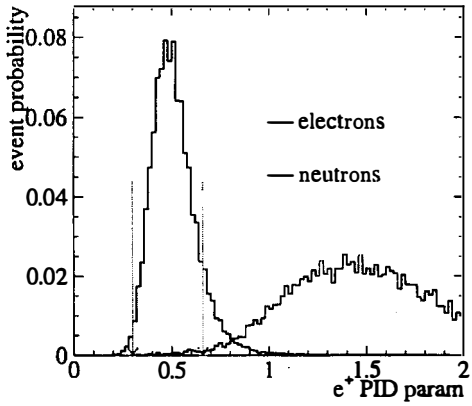

Figure 1: Particle ID parameter for electrons and neutrons. The arrows indicate the positions of the cuts for this analysis.

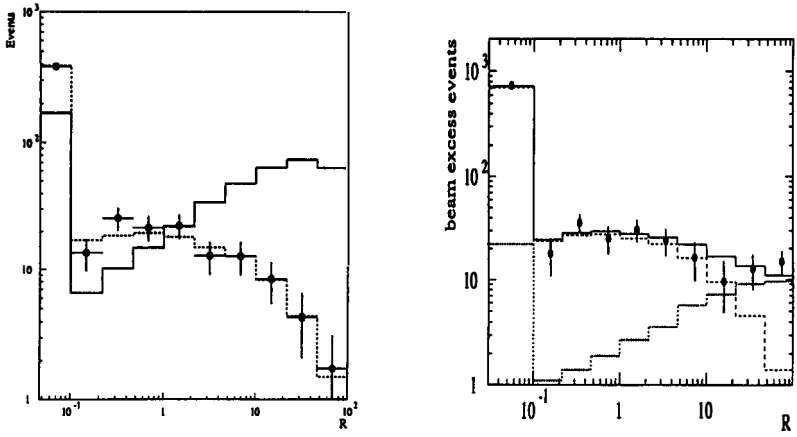

Figure 2: The R distribution for the $\nu_e^{12}C_{g.s.}$ sample is on the left. In this plot the dashed histogram is the distribution if the γs are taken to be entirely uncorrelated, and the solid is the distribution if the γs are taken to be entirely correlated. The R distribution for the DAR sample is shown on the right. In this plot the dotted histogram is the correlated component while the dashed is the uncorrelated component, and the sum is the solid histogram. Points with error bars are the data in both plots.

Separation of correlated neutron-capture photons from the accidental signals is achieved using an approximate likelihood ratio R [7, 2] for the correlated and accidental hypotheses. R discriminates between correlated and accidental photons by exploiting the quite-different distributions in three variables: the time and distance between the reconstructed photon and $e^{\pm}$ vertices and the tank hit multiplicity distribution of the photon. Figure 2 shows the R distribution for a $\nu_e{}^{12}C_{g.s.}$ sample in which one expects there to be no correlated photon (since no neutron is produced in the reaction), and the facing figure shows the DAR R distribution. From the second plot one deduces the number of events in the DAR sample which have correlated gammas and thus satisfy the conditions to be oscillation signature events. This is one way in which one may count oscillation events. The other is to simply cut at a large value of R, above which one has a high purity oscillation candidate sample, and count the events which survive. We do the former to calculate the oscillation probability in order to take advantage of the bigger efficiency, while the latter sample may be used for the purpose of making distributions of energy, position, etc.

Figure 3 shows the energy distributions of the $e^{\pm}$ samples with no R requirement and with $R > 30$. An excess is clearly visible in figure 3b. The facing plot in that figure shows the same distribution, but now including all of the data from 1993-1997. This plot is **preliminary**. One sees from it that the data favours low Δm^2, although higher Δm^2 cannot be completely ruled out.

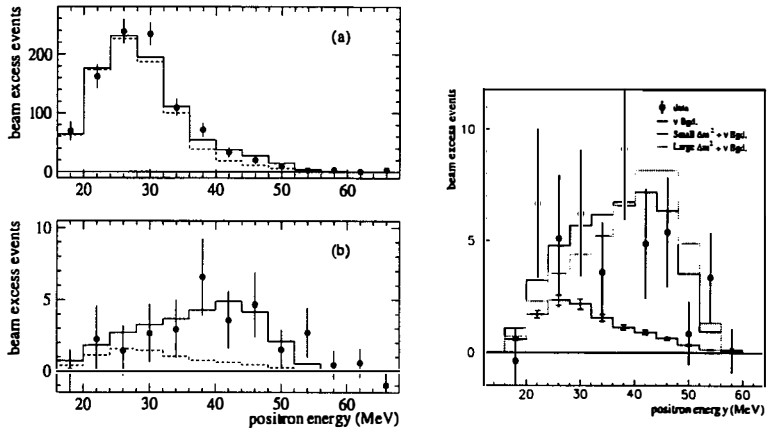

Figure 3: The 1993-1995 e^+ energy distribution for events with (a) $R \geq 0$ and (b) $R > 30$. Shown in the left figures are the beam excess data, estimated neutrino background (dashed), and expected distribution for neutrino oscillations at large δm^2 plus estimated neutrino background (solid). The right plot shows the **preliminary** 1993-1997 e^+ energy distribution for events with $R > 30$. (Compare to figure (b).) Note the small sizes of the error bars on the background.

The increase in statistics in the 1993-1997 data allows for further systematic checks. One check that may be performed is to investigate the possibility of events in our oscillation sample which contain greater than one photon. The existence of such events might signal the presence of beam-related neutrons. One would expect such neutrons to be energetic enough that, if present, the ratio of events with multiple correlated gammas to events with just one correlated gamma should be approximately 0.60. Table 1 is a **preliminary** table which shows, in both of the energy ranges which are used in reference [2], that no such events are in the DAR sample. This is the third such cross-check [2] which rules out beam-related neutrons.

Table 1: Events with multiple correlated ($R > 30$) gammas. This is **preliminary** and demonstrates the absence of beam-related neutrons in the DAR sample.

Energy Range	# gammas/Ratio	beam-on	beam-off	Excess
$20 < E_{e^\pm} < 60$				
	$\#\gamma = 1$	61	259	45.4 ± 7.9
	$\#\gamma > 1$	6	87	0.8 ± 2.5
	Ratio	0.10	0.34	0.02 ± 0.06
$36 < E_{e^\pm} < 60$				
	$\#\gamma = 1$	29	90	23.8 ± 5.4
	$\#\gamma > 1$	1	36	-1.2 ± 1.1
	Ratio	0.03	0.40	-0.05 ± 0.05

3 Analysis: DIF

The e^- which is produced in the tank from the higher energy ν_e flux requires a more robust PID algorithm than required in the DAR analysis. Such ID is provided by a likelihood technique, in which the measured time and charge on each tube in a selected event is compared against its predicted time and charge. The most likely configuration – vertex, direction and energy of each postulated electron – with respect to the measured quantities is calculated using measured physical properties of the tank and the tubes.

The likelihood value of the event itself, as well as quantities such as the ratio in the event of Čerenkov to scintiallation light, provide discrimination against electromagnetic background, while other event variables, such as extrapolated track distance back to the tank wall provides discrimination against non-electromagnetic backgrounds, such as π^0s and ns from cosmic-ray induced activity entering the tank. See figure 4.

The energy distribution for the finale sample of events is seen in figure 5.

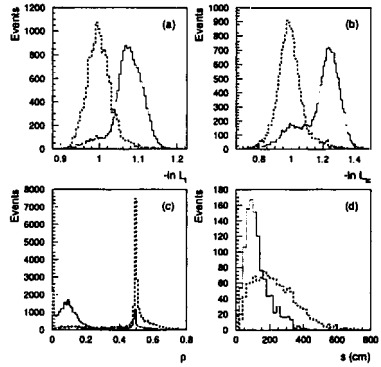

Figure 4: Timing likelihoods for (a) the entire event and (b) the Čerenkov region only. (c) is the Čerenkov-to-scintillation density ratio, ρ, while (d) is the projected track-length to the tank wall. (a)-(c) correspond to all (beam on+off) DIF data after some pre-selection [1], while (d) corresponds to this same event sample but after all other cuts were applied. Solid is data, dashed is MC normalized to the same area.

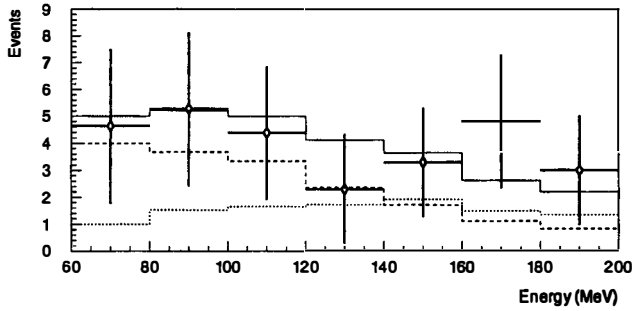

Figure 5: The energy distribution (points with error bars) for the final beam-excess DIF events. The expectation for backgrounds (dotted histogram), the oscillation signal for large values of δm^2 (dashed histogram) and the some of the two (solid histogram) are shown also.

4 Results

A 99% likelihood allowed region (DAR analysis) is shown in figure 6 compared with the 95% confidence region from the DIF analysis. The DIF and DAR analyses give consistent allowed regions and oscillation probabilities. Table 2 shows the results of the DIF and DAR analyses. Papers providing further details on these two analyses may be found in [8].

A global analysis in which both the DAR and DIF νs are treated with the same fitting algorithm and in which all the data from 1993-1997 is included is underway.

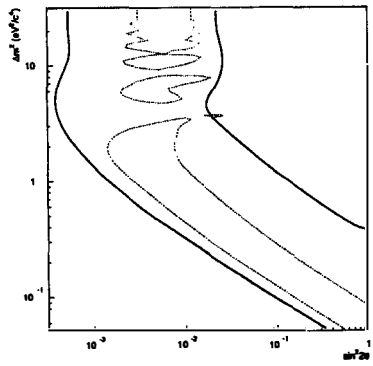

Figure 6: The allowed regions in $\sin^2\theta - \Delta m^2$ from the DAR (dashed) and DIF (solid) analyses.

Table 2: Results of the analyses. In the case of the DIF (DAR) analysis results from the sample corresponding to the logical OR [1] (Selection VI [2]) are shown. The total number of events, background, Excess, efficiency and oscillation probability are shown.

Data	Beam on	Bgd.	Excess	eff. (%)	osc'n. prob. (%)
DIF, "OR"	40	21.9 ± 2.1	18.1 ± 6.6	16.5	0.26 ± 0.10
DAR, "VI," $R > 30$	22	4.6 ± 0.6	17.4 ± 4.7	8.5	0.31 ± 0.13

References

[1] C. Athanassopoulos *et al.* (LSND Collaboration),
LA-UR-97-1998/CRHEP-E191;nucl-ex/9709006.

[2] C. Athanassopoulos *et al.* (LSND Collaboration), Phys. Rev. **C54** 2685 (1996).
C. Athanassopoulos *et al.* (LSND Collaboration), Phys.Rev.Lett. **77** 3082 (1996).

[3] C. Athanassopoulos, *et. al.*, Nucl. Inst. and Meth. A **388** 149 (1997).

[4] C. Athanassopoulos *et al.* (LSND Collaboration), Phys.Rev. **C56** 2806 (1997).

[5] C. Athanassopoulos *et al.* (LSND Collaboration), Phys. Rev. C **55,** 2078 (1997).

[6] J. J. Napolitano *et. al.*, Nucl. Inst. and Meth. A **388** 149 (1997).

[7] C. Athanassopoulos *et al.* (LSND Collaboration), Phys. Rev. Lett. **75**, 2650 (1995).

[8] *http://www.neutrino.lanl.gov.*